SCIENTIFIC REPORTS

OPEN

SUBJECT AREAS:
TOPOLOGICAL INSULATORS
ELECTRONIC PROPERTIES AND MATERIALS
MAGNETIC PROPERTIES AND MATERIALS
FERROELECTRICS AND MULTIFERROICS

Received
18 April 2013

Accepted
6 June 2013

Published
21 June 2013

Correspondence and requests for materials should be addressed to P.A. (pushan@tifr.res.in)

Multiferroic Behavior in Elemental Selenium below 40 K: Effect of Electronic Topology

Anirban Pal[1], Sharmila N. Shirodkar[2], Smita Gohil[1], Shankar Ghosh[1], Umesh V. Waghmare[2] & Pushan Ayyub[1]

[1]Department of Condensed Matter Physics & Materials Science, Tata Institute of Fundamental Research, Mumbai 400005, India, [2]Theoretical Sciences Unit, Jawaharlal Nehru Centre for Advanced Scientific Research, Bangalore 560064, India.

The quasi-one-dimensional, chiral crystal structure of Selenium has fascinating implications: we report simultaneous magnetic and ferroelectric order in single crystalline Se microtubes below ≈40 K. This is accompanied by a structural transition involving a partial fragmentation of the infinite chains without losing overall crystalline order. Raman spectral data indicate a coupling of magnons with phonons and electric field, while the dielectric constant shows a strong dependence on magnetic field. Our first-principles theoretical analysis reveals that this unexpected multiferroic behavior originates from Selenium being a weak topological insulator. It thus exhibits stable electronic states at its surface, and magnetism emerges from their spin polarization. Consequently, the broken two-fold rotational symmetry permits switchable polarization along its helical axis. We explain the observed magnetoelectric couplings using a Landau theory based on the coupling of phonons with spin and electric field. Our work opens up a new class of topological *surface-multiferroics* with chiral *bulk* structure.

Multiferroic materials in which ferromagnetism and ferroelectricity not only coexist but are intrinsically coupled are of great technological interest and have been a subject of intense research[1–3]. Biferroic behavior has so far been seen in either low-symmetry, complex oxides[4] or composite multiphase materials[5–7].The mutually exclusive nature of ferromagnetism and ferroelectricity is ascribed to symmetry restrictions as well as conflicting chemical requirements[8]. A possible solution is offered by systems in which different ions or functional groups are responsible for different types of ferroic order. In such 'Type-I' multiferroics, magnetism and ferroelectricity originate independently from different sublattices (*e.g.*, $BiFeO_3$[9,10]) and necessarily exhibit a weak coupling. In 'Type-II' multiferroics, on the other hand, ferroelectricity is induced by certain types of non-collinear (*e.g.*, cycloidal) spin order that breaks inversion symmetry. Such systems (that include certain rare earth manganites[11,12]) show an *intrinsic* coupling between the ferroelectric and magnetic order parameters[13,14].

Very recently, a particularly interesting connection has been suggested between multiferroic systems and topological insulators[15,16]. The geometric part of the orbital magnetoelectric coupling in 3-dimensional topological insulators has been shown to be analogous to polarization or the geometric phase of 1-D topological insulators. While the former relates to Chern-Simons 3-form, the latter corresponds to Chern-Simons 1-form, and hence these properties are quantized in topological insulators. These novel ideas are yet to be demonstrated experimentally through identification of topological insulators exhibiting magneto-electric coupling. It is relatively simpler to think of a 3-D insulator with quasi-1-D structure of special symmetry that would exhibit a quantized polarization, and hence a surface charge. A possible spontaneous magnetic ordering of this surface charge can potentially give rise to interesting types of magnetoelectric coupling under certain symmetry conditions, and is shown here to manifest in one of the simplest materials, elemental selenium.

Even though the earliest known elemental semiconductor and photoconductor, Se[17], has an unusual, quasi-one-D, chiral structure, it has attracted little attention as a potential multiferroic. The crystal structure of trigonal Se (space group $P3_121$) consists of parallel, helical atomic chains with three atoms per unit cell. The atoms within a helix are covalently bonded, and the weakly coupled helical chains are arranged on a hexagonal lattice. With a 4 s^2p^4 configuration, Se was so far believed to be an insulator with no magnetic ordering[18,19]. We have, however, found evidence for both magnetic and ferroelectric order in Se microtubes below ≈40 K. Both our experimental and theoretical studies suggest that the magnetic ordering occurs mainly at the crystal surface. Further, though bulk Se is insulating, our electronic structure calculations show metallic behavior at its surface, which is shown to

originate from a nontrivial topology of electronic states of bulk Se. This explains why the phenomenon was missed earlier in bulk Se, while we succeeded in capturing it in samples of reduced dimensionality. The complex, chiral structure and consequent non-trivial electronic topology of Selenium are ultimately responsible for the unprecedented observation of multiferroic order in an *elementary* system. This obviously suggests that other materials with similar structure should also be investigated for multiferroic behavior.

Results

Observation of magnetization and electrical polarization in Se. Our studies involved perfect single crystals of Se in the form of hexagonally-faceted, hollow microtubes: ≈5 mm long and 50–300 μm in diameter (Fig. 1(a)), grown by vapor transport with an amorphous Se pellet (99.999%) as precursor. The X-ray diffraction pattern matched perfectly with trigonal Se (Fig. 1(b)), while transmission electron microscopy showed excellent crystalline order (Fig. 1(c)) and no surface contamination. Energy dispersive X-ray analysis indicated 100% Se and X-ray fluorescence analysis showed about 1% Sulfur, but no other impurities down to a detection limit of 10–100 ppm.

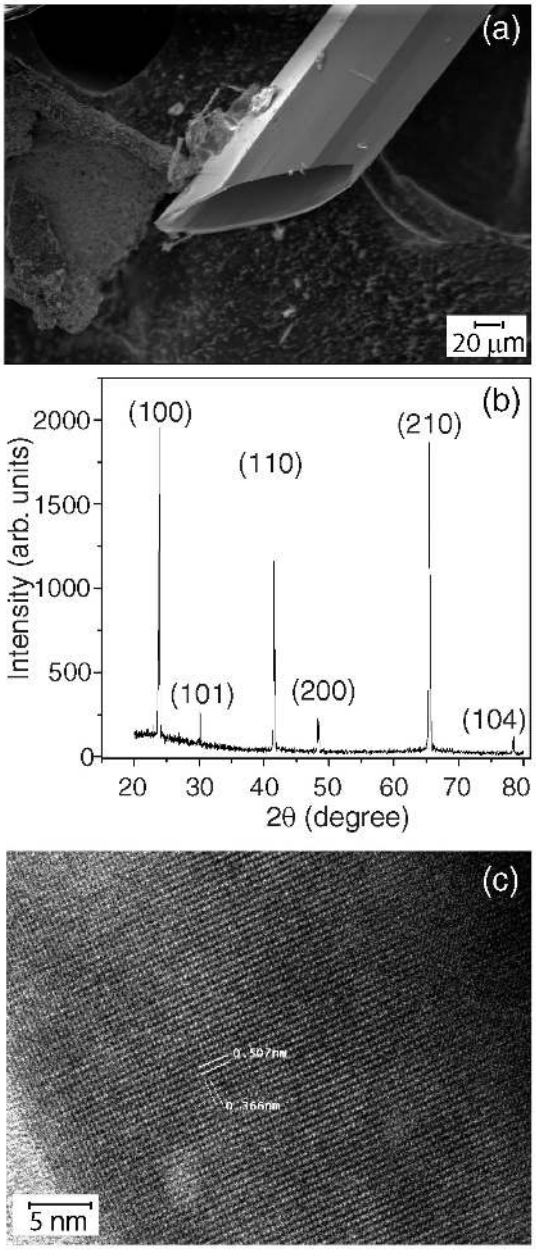

Figure 1 | (a) Scanning electron micrograph of a typical, faceted, hollow microtube of Se, (b) X-ray diffraction pattern and (c) high resolution lattice image (TEM) showing perfect single crystalline order.

Magnetic hysteresis measurements were performed in the 2–100 K range on a bunch of ≈10 microtubes with field parallel to the long axis of the rods. At 2 K, the samples showed complete saturation of magnetization, with the M-H curve indicating either antiferromagnetic or weak (canted) ferromagnetic behavior (Fig. 2(a)). The saturation of magnetization gradually disappears with increasing temperature. The temperature dependence of the saturation magnetization (Fig. 2(b)) indicates a transition temperature near 40 K, also supported by Raman data. Ferroelectric hysteresis measurements were carried out with the sample dipped in liquid N_2 and liquid He, to negate the effect of heating caused by the large applied voltage. At 4.2 K, the data clearly indicate polarization saturation and hence ferroelectric order (Fig. 2(c)). At 77 K, the sample exhibited large area loops expected from a lossy dielectric. An expanded view of the 4 K data (Fig. 2(c), inset) supports the ferroelectric nature of the ordering. The increase in the dielectric loss at higher temperature (well above T_C) occurs because Selenium is a semiconductor. At low temperatures (in the ferroelectric phase), it is basically insulating. As the temperature rises, charge carriers are increasingly available in the conduction band, as reflected in the observed lossy hysteresis loop at 77 K. Capacitance measurements at different frequencies with voltage applied parallel to the rods show a prominent peak at ≈ 40 K (Fig. 2(d)), which indicates the ferroelectric ordering temperature. Up to 80 kHz, these data remain essentially unchanged, as dielectric dispersion effects are expected only at higher frequencies. Further confirmation is provided by pyroelectric measurements performed by first cooling the Se microtubes in an electric field applied along the c-axis, followed by a measurement of the temperature dependence of the absolute charge. We observed a clear, reversible pyroelectric signal below ≈ 50 K (Supplementary Information: Fig. S1). Both the ferroelectric loop and the pyroelectric signal are somewhat asymmetric with respect to the polarity of the applied field. This indicates a history dependence which is discussed later.

Observation of spin-charge-lattice (phonon) coupling. Crucial insights pertaining to the spin-charge-lattice coupling – central to the nature of the multiferroic behaviour – are provided by Raman spectroscopy. At 300 K, we observed a single intense mode at 232 cm^{-1} (Fig. 3, bottom), which has been identified as the E phonon in trigonal Se[20]. However, at 4 K, we also observed intense modes in the 400–750 cm^{-1} region. The extended nature of these modes and the multiple features associated with them indicate that they arise from higher order, non-phononic elementary excitations – which we believe to be magnons. These modes are resonantly enhanced at 647.1 nm and barely observable at other wavelengths (Supplementary Information: Fig. S2). We could confirm the magnonic origin of these modes by simply applying an external magnetic field: even a relatively small field (≈0.1 kOe) severely distorted these modes, while the phonon mode was not affected. The shaded regions in Fig. 3 show the imaginary part of the Raman response function: $\chi''(\omega) \sim I(\omega)/[1 + n(\omega)]$ at different temperatures ($I(\omega)$ = Raman scattering intensity, ω = Stokes shift and the Bose factor, $n(\omega) = 1/[\exp(\hbar\omega/kT) - 1]$). The area under the magnon spectrum shows rapid extinction in the 30–50 K range (Fig. 4(a)), though weak magnetic fluctuations probably persist until 100 K, consistent with the temperature dependence of the magnetization (Fig. 2(b)). This supports our assignment of these high frequency spectral features to higher order magnon modes. It is important to reiterate at this point that all our data indicate that – within experimental uncertainty - the magnetic and ferroelectric transition temperatures are practically coincident (40±10 K).

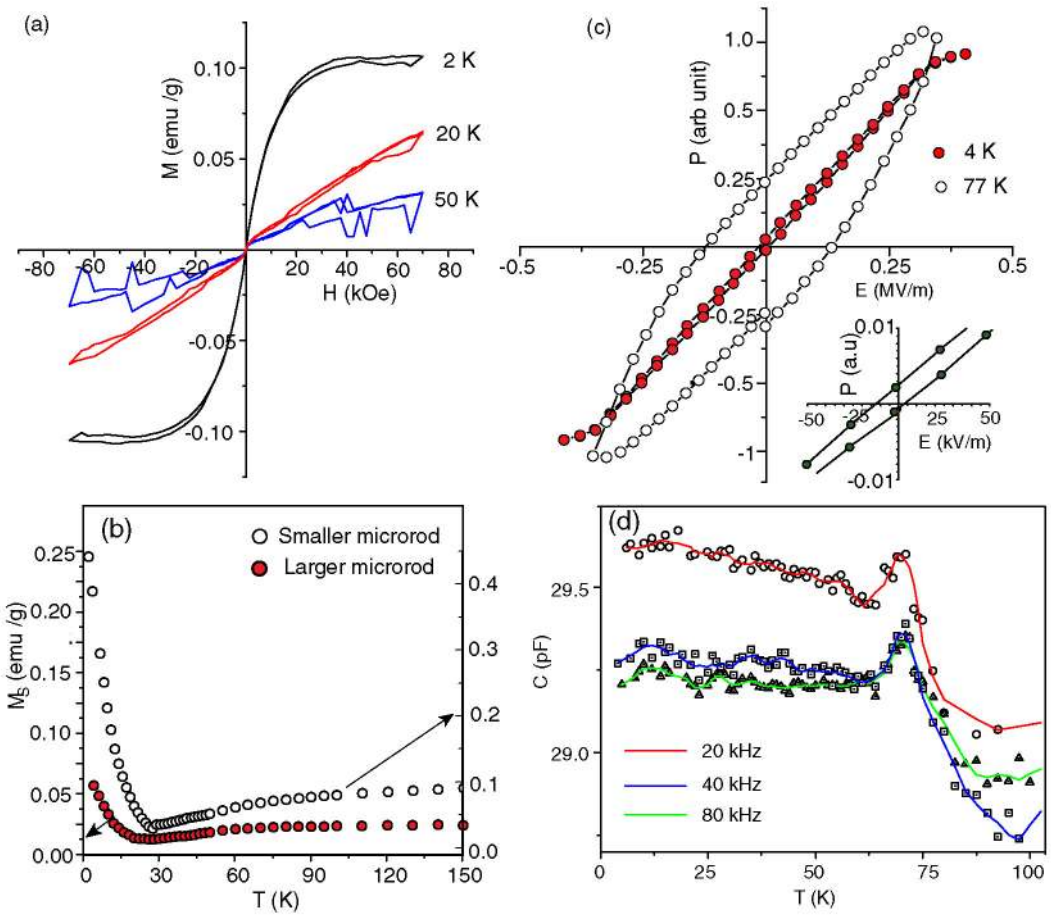

Figure 2 | (a) Magnetic hysteresis curves for a bunch of parallel Se microrods at three temperatures spanning the magnetic ordering temperature. (b) Temperature dependence of the saturation magnetization, M_S, (measured at 5 T) for two samples of Se microtubes with average outer diameters of 80 μm and 250 μm. Clearly, M_S increases with the specific surface area of the sample. (c) Ferroelectric hysteresis curve for Se microrods at 4 K (solid dots), clearly indicating polarization saturation. An expanded view near the origin is shown on right. Similar data recorded at 77 K represents behavior typical of a lossy dielectric. The frequency of the applied ac field was 10 kHz. Note that Se exhibits a negative temperature coefficient of resistance. (d) Temperature dependence of the capacitance (dielectric response) recorded at three different signal frequencies (20, 40 and 80 kHz) and at zero magnetic field.

The possibility of magnetoelectric coupling was probed by applying a dc electric field normal to the Se microrods, using a specially fabricated holder. Fig. 4(b) shows that the magnon frequencies are strongly affected by the applied field, while the phonon frequency remains almost constant (Supplementary Information: Fig. S3). Further, the magnon frequency shift changes sign with the electric field direction. This important observation (along with the magnetic field dependence of the dielectric response) is an unambiguous manifestation of the coupling between the charge and spin order parameters. Magnetoelectric coupling in the system is conclusively proven by the magnetic field dependence of the dielectric response: the peak in the dielectric response disappears in an applied magnetic field of 2 T (Fig. 4(c)). The Raman data provides another significant input: the phonon mode intensity falls sharply in the vicinity of the magnetic transition temperature, though it does not vanish (Fig. 4(a)). This indicates a strong spin-phonon coupling in the system.

The relatively low value of the saturation magnetization of the Se microtubes ($M_S \approx 10^{-3}$ μ_B/atom at 2 K) indicates a surface origin (note that 0.1–0.01% of the Se atoms reside on the tube surface). This is corroborated by our observation that for two samples with different average tube diameters, M_S scales roughly with the specific surface area (Fig. 2(b)).

First-principles theory of electronic structure and topology of Se. We now discuss the possible origin of the surface moments in the Se microstructures. Our first-principles calculations based on density functional theory (DFT) with generalized gradient approximation (GGA) to exchange correlation energy estimate the structural parameters: a = 4.47Å and c = 5.04Å, within 3% of their reported values[21]. We find an indirect band gap of 1.1 eV, which is underestimated with respect to the experimental value[22] by ≈41% (a known limitation of the DFT method). For bulk Se, our calculations with local spin or magnetic moments on Se sites initialized with ferromagnetic (FM) and antiferromagnetic (AFM) ordering resulted in a state with vanishing magnetic moments, confirming our earlier prediction[19] that bulk Se is non-magnetic.

We next investigated the possible presence of magnetic moments in 2–8 atom, helical chains of Se, initialized with different types of magnetic order along the chains. For all except the 3-atom chains, the self-consistent electronic ground state clearly exhibits an ordering of magnetic moments, with the moments confined to the ends of the chains (Supplementary Information: Fig. S4). For odd-atom chains, the initial AFM state de-evolved into a FM state, while even-atom chains exhibit stable ordering of both AFM and FM types, with very similar energies. This supports our contention that the observed magnetism originates from the surface or boundary. In this connection, the appearance of a weak Raman line at ≈250 cm^{-1} (Fig. 3) at low temperatures is significant. It indicates the nucleation of the α-monoclinic structure[23] as a minority phase within the (majority) trigonal structure. Evidence for the partial nucleation of this

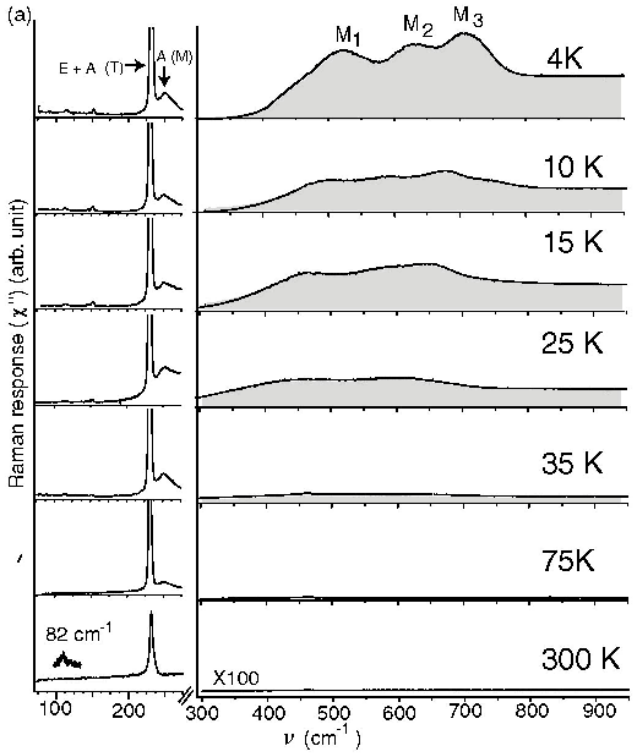

Figure 3 | Raman scattering response function from Se microrods at seven temperatures spanning the magnetic ordering temperature. The room temperature spectrum is at the bottom. The shaded regions in the 4 K–35 K spectra represent the magnon contribution.

α-monoclinic phase at low temperatures is also seen in temperature-dependent XRD measurements. We propose that these small, second phase nuclei merely act as somewhat extended point defects and cause the fragmentation of the infinite helical chains of trigonal Se into shorter fragments, without an overall loss of crystal symmetry.

To simulate the (0001) surface, we studied slabs consisting of 10 and 11 atomic planes separated from its periodic images by a vacuum of 1 nm along *c*-direction and initialized with AFM and FM ordering of spins at its surface. The non-magnetic state of the slab exhibits a metallic electronic structure (Fig. 5(a)), and the bands crossing the Fermi energy are localized at the surfaces. As Se is quasi-one-dimensional, we expect this electronic structure to be unstable possibly with respect to magnetic ordering. Keeping in mind that magnetism in graphene nano-ribbons arising from its edge states is stabilized by on-site correlation[24], we simulated the Se slab by including on-site correlation with Hubbard $U = 1$ eV to 5 eV, and initial states with AFM and FM ordering. For all the Hubbard *U* values, magnetic moments and the nature of electronic structure (with band gap increasing with *U*) of the selenium slab remain qualitatively the same (see Supplementary Information: Fig. S5). In contrast to bulk Se, the self-consistent solution exhibits nonzero (~0.5 μ_B/atom) local magnetic moments on the surface atoms even after structural relaxation. The relaxed structures with AFM and FM configurations are energetically the same, implying only a weak interaction between the moments at the opposite slab-surfaces. A band gap opens up in the electronic structure upon magnetic ordering at the Se slab surfaces (Fig. 5(b) and (c)), and the visualization of the spin-density iso-surfaces (Figs. 5(d) and (e)) clearly shows that the surface states are responsible for the magnetic character of the slabs. An increase in the on-site correlation energy *U* results in further stabilization of the surface spins and their ordering.

The robustness of the surface states of the Se slab and their resemblance to the localized states at the end of single helical chains of Se

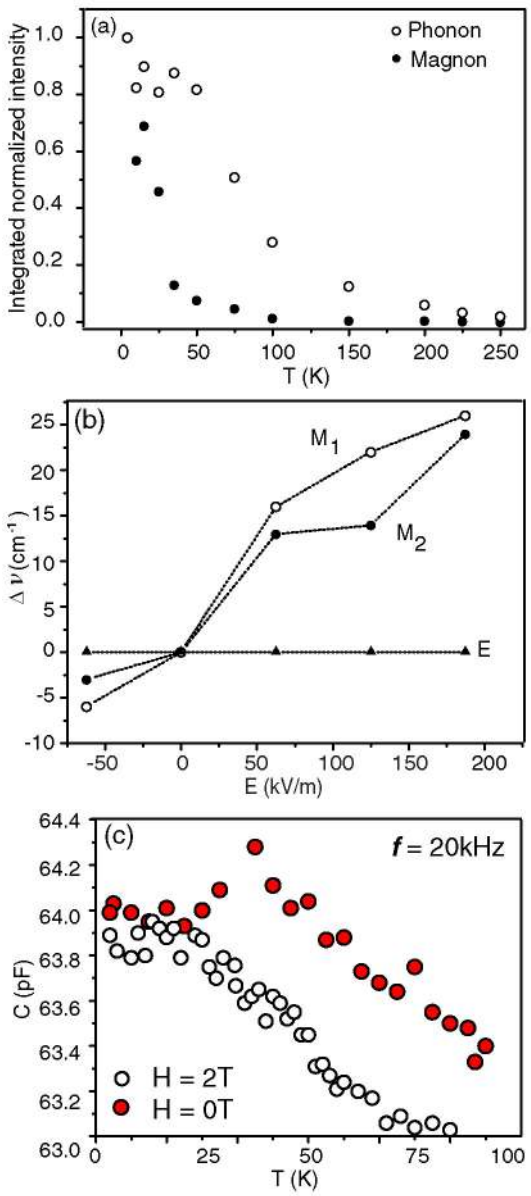

Figure 4 | (a) A plot of the temperature dependence of the (normalized) area under the respective spectral response functions shows that the magnon mode response drops sharply near the magnetic transition temperature (30–50 K), while the phonon mode is partially damped. (b) Shift in the magnon mode frequencies (M_1 and M_2) with applied dc electric field, recorded at 4 K. The phonon frequency shows very little field dependence. (c) Temperature dependence of the capacitance (dielectric response) in zero magnetic field (red dots, upper curve) and in an applied magnetic field of 2 T (open circles, lower curve) confirms magnetoelectric coupling.

prompt us to trace their origin to the electronic topology[25] of bulk Se. As Se has a quasi-one-dimensional structure, we note that the relevant topological invariant is essentially the Berry phase of occupied electronic states, which is essentially the polarization[26]. Symmetry considerations predict zero polarization in the *ab* plane as well as along the *c*-axis of bulk Se. Berry-phase calculations confirm the former expectation but predict a half-integer quantum polarization, $P_z = e/A$ along z-axis (e = electronic charge, A = unit cell area). This does not violate symmetry principles, since polarization – as a Berry phase – can be estimated only within an integer quantum polarization. Thus, P and $-P$ (obtained by applying inversion symmetry or a

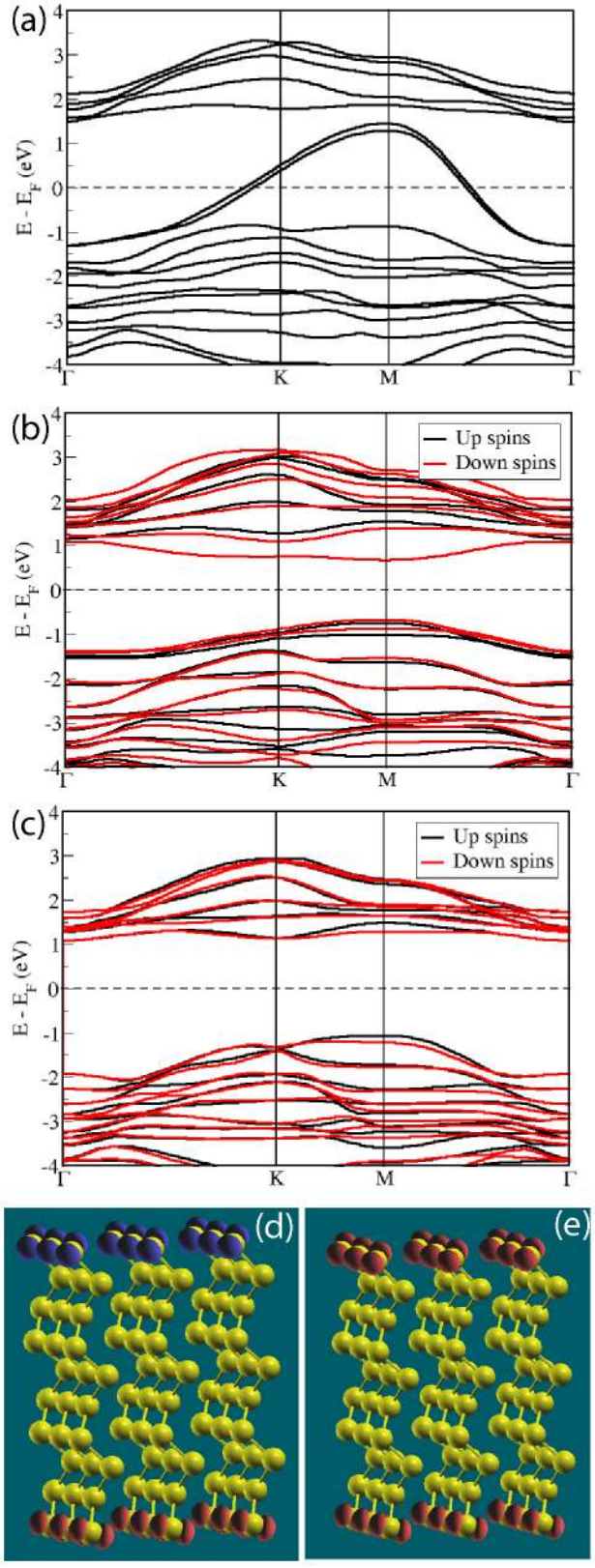

Figure 5 | Electronic structure of Se (0001) slab with 10 atomic planes in (a) a non-magnetic configuration with metallic nature due to surface states, (b) ferromagnetic configuration, and (c) antiferromagnetic configuration obtained with U = 5 eV, exhibiting a bandgap. Iso-surfaces of spin-density in (d) antiferromagnetic configuration and (e) ferromagnetic configuration, revealing the magnetic moments localized at the surface.

two-fold rotation along an axis in the *ab*-plane in case of Se) may differ by an integer quantum; hence a half-integer quantum polarization is allowed by symmetry even in centrosymmetric systems[27]. We believe bulk Se is the only system known so far to exhibit a half-integer quantum *electronic* polarization (*i.e.* the electronic structure of bulk Se has an overall Berry phase of π) and its total (ionic + electronic) polarization remains invariant upon any shift in origin. This would naturally support electronic charge at the surfaces and consequently the magnetism. Ordering of spins at the surface breaks the two-fold symmetry of Se (see Figure 5) and gives rise to a switchable polarization. This *necessarily* implies that the ferroelectric and magnetic ordering temperatures are identical, in conformity with our experimental observations. Such magnetically induced polarization, though small, *inherently* involves a strong magnetoelectric coupling[28]. We point out that Se is a *weak* topological insulator (TI), being a 2-D array of 1-D insulators with nontrivial topological invariant. This is reflected in an even number of band crossings at the Fermi energy (Fig. 5) in the electronic structure of the non-magnetic state. As a result, its surface states are not as robust against disorder as those of a *strong* 3-D TI. Finally, as the topological invariant of bulk Se is linked to its structure and forced by its symmetry, it can be considered a *crystalline TI*[29].

Origin of the magnetoelectric effect: spin-charge-phonon coupling. To understand the unusual Raman spectra observed by us, we now present an analysis of the phonons and their coupling with spin and electric field. Our theoretical estimates of the phonon frequencies of bulk Se (217 cm^{-1} for the E mode and 89 cm^{-1} for an IR-active A_2 mode) are in reasonable agreement with observations (232 cm^{-1} and 82 cm^{-1}, respectively). The Hellman-Feynman forces on Se atoms in the non-magnetic state with atomic structure obtained by minimizing energy of the ferromagnetic state give the lowest order spin-phonon coupling. Projecting these onto the phonon eigenvectors, we establish that the Raman-active *E* mode at 217 cm^{-1} exhibits the largest spin-phonon coupling and the lower energy *E* mode at 128 cm^{-1} shows noticeable coupling with spin. This spin-phonon coupling is responsible for the concurrent anomalies in magnon and phonon modes seen in the Raman spectra near the magnetic ordering temperature. A weak structural distortion (implied by the appearance of a low intensity Raman A_1 mode at low temperatures, see Fig. 3) at the magnetic/ferroelectric transition can be also ascribed to the spin-phonon coupling. Though the three Se atoms in the trigonal crystal cell are symmetry equivalent and homopolar, an external electric field *does* couple to its lattice (phonons) due its non-trivial symmetry (see Table I). The tensorial character of the coupling of electric field with the atomic displacements (Born dynamical charges) permits a nonzero charge Z for Se atoms positioned on the x-axis, with the electric field also along x-axis, *e.g.*, $(Z)_{xx} = 0.70$.

Having established the coupling of phonons with spin and electric field based on experimental and first-principles theoretical evidence, we express free energy of Se surface as a function of spin (*S*), phonon coordinate (*u*) and electric field (*E*), using a Landau-like theory: $F = \frac{1}{2}Ku^2 - ZEu - LSu + JS^2$, where $K = \mu\omega^2$ is the phonon spring constant, *Z* is the dynamical charge, *L* is the spin-phonon coupling and *J*, the exchange coupling. Minimizing energy with respect to *u*, we obtain the effective free energy: $F_{eff} = -\frac{Z^2}{2K}E^2 + \left(J - \frac{L^2}{2K}\right)S^2 - \frac{ZL}{K}ES$, where the three terms are, respectively, the phonon contribution to the dielectric constant, the phonon-renormalized exchange coupling and the phonon-mediated linear magnetoelectric coupling. We note that magnon frequency is determined by the effective exchange coupling.

Since this linear theory does not explain the electric field dependence of magnon frequency (a third order effect), we consider the third order coupling of a phonon with the electric field: $H = \alpha u^2 E$,

Table I | (Top) The mode effective charges (Z^m) of Raman active E mode of bulk Se with an undistorted structure. (Centre, Bottom) Changes in the mode effective charges ($Z^m_{distorted} - Z^m_{undistorted}$) of a distorted structure obtained by freezing in the atomic displacements of the relevant Raman active E modes

	Mode effective charges of undistorted structure		
Mode frequency (cm^{-1})	*X*	*y*	*z*
128	0.142	1.293	0.000
128	1.293	−0.142	0.000
217	0.016	−0.117	0.000
217	0.117	0.016	0.000
	Change in mode effective charges on freezing E mode at 128 cm^{-1}		
	x	*y*	*z*
128	−0.090	0.004	0.017
128	0.028	−0.093	−0.006
	Change in mode effective charges on freezing E mode at 217 cm^{-1}		
	x	*y*	*z*
217	0.027	0.018	−0.046
217	−0.017	−0.031	0.021

with $\alpha = -\frac{\partial Z}{2\partial u}$. We determine α by distorting the structure with the atomic displacements (u) by ≈1% of the lattice constant and estimating the Born dynamical charges of phonons using DFT linear response. Interestingly, lower energy modes exhibit the strongest third order coupling with electric field, while α of the Raman-active *E* mode is relatively much weaker (see Table I), which explains the observed independence of the *E* mode on electric field. The exchange coupling, renormalized by lower energy modes, can be shown to change with electric field as: $\frac{L^2}{2K}\left(1-2\frac{\alpha E}{K}\right)$. In this model, the observed dependence of magnon frequency on electric field originates from the third order phonon--electric field and linear spin-phonon couplings. Similarly, dielectric constant varies linearly with magnetic field and the magneto-capacitance is proportional to: $ZL\alpha \Big/ \left[2J\left(K-\frac{L^2}{2J}\right)^2\right]$.

Discussion

We have established the existence of ferromagnetic order in Se microrods below ≈40 K from bulk magnetization and magnon scattering data. Ferroelectric order in a similar temperature range is indicated by a peak in the dielectric response near T_C, reversible spontaneous polarization (evidenced by pyroelectric response on field reversal), and ferroelectric hysteresis, with a clear tendency towards saturation. We point out that the possible existence of piezoelectricity with fairly high electromechanical coupling had already been suggested some time back[30]. Magnetoelectric coupling is clearly indicated by our data on the magnetic field dependence of the dielectric response and the electrical field dependence of the magnon mode frequencies.

While the possibility of magnetoelectric coupling at the surface of magnetic metals has recently been pointed out[31], the emergence of multiferroic behavior in a *non-magnetic*, elemental semiconductor is certainly quite astonishing. Indeed, ferroelectricity and magnetism are neither expected, nor observed in bulk Se. Our work suggests that the chiral arrangement of Se atoms leads to a coupling between the lattice and electric field, while the spin-polarized surface arises from its unique electronic structure with non-trivial topology, reflected in a Berry phase of π. This highly unusual coupling of its lattice with the electric field, surface spins or magnetic excitations allows *elemental* Se to acquire multiferroic properties, observable only in low-dimensional samples. The *surface* origin of the phenomenon necessarily implies that the volume-normalized polarization and magnetization do not appear very large. Interestingly, the multiferroic transition appears to be associated with the nucleation of a small fraction of the α-monoclinic phase (in which the Se atoms are arranged in 8-member rings, rather than long chains), that increases with decreasing temperature below T_C. We suggest that dispersed nuclei of this minority phase effectively break up the infinite 1-D chains of the majority trigonal phase into shorter lengths, thus maximizing their number, but not affecting the overall crystalline order. This model also explains the history dependence, e.g., in the pyroelectric data, since cooling the sample below T_C would each time produce a different realization of the geometric arrangement of the short chains. Significantly, our work uncovers a new route to multiferroic behavior that is not strongly restricted by symmetry, and indicates that similar magneto-electric surface properties could well emerge in other semiconductors with low-symmetry chiral space group. At the same time, our observations provide strong experimental support to the recent theoretical investigations that propose electronic topology as a novel origin of magnetoelectric coupling.

Methods

Magnetic measurements were made in a Quantum Design SQUID magnetometer. Raman spectra were recorded in the backscattering geometry with incident polarization parallel to the micro-rod axis, using a Jobin-Yvon T-64000 triple grating spectrometer with a Kr laser 647.1 nm excitation. Dielectric (capacitance) measurements were carried out in a He cryostat (uniformly illuminated through an optical window) by placing the Se microtubes on a 10 mm × 8 mm Sapphire substrate. Ferroelectric hysteresis measurements were made by sandwiching the microtubes between two 6 mm diameter copper plates specially customized for low temperature measurements. In both cases, contacts were made with low temperature Silver paste. First-principles calculations were based on density functional theory (DFT) as implemented in the Quantum ESPRESSO[32] package with spin-density dependent generalised gradient approximation (GGA) to exchange-correlation function (Perdew, Burke and Ernzerhof[33]) and ultrasoft pseudopotentials[27] to represent the interaction between ionic cores and valence electrons. Spin polarized calculations were performed using the GGA + U method[34] with U = 1 eV to 5 eV. Electric polarization was determined using the Berry's phase approach[35]. Occupation numbers were smeared using a Fermi-Dirac scheme with a broadening of 0.005 Ry. For GGA calculations, Kohn-Sham wavefunctions were represented with a plane wave basis with an energy cutoff of 50 Ry and kinetic energy cutoff for charge density of 400 Ry. Integration over the Brillouin zone was carried out using the Monkhorst-Pack scheme with regular 5 × 5 × 5 and 6 × 6 × 1 meshes of **k**-points for bulk and slab calculations, respectively. Some of the subtle results (e.g., Berry phase polarization) were reproduced with LDA[36], and HGH pseudopotentials[37] and energy cutoff of 70 Ry using ABINIT package[38,39].

1. Wang, K. F., Liu, J.-M. & Ren, Z. F. Multiferroicity: the coupling between magnetic and polarization orders. *Adv. Phys.* **58**, 321–448 (2009).
2. Eerenstein, W., Mathur, N. D. & Scott, J. F. Multiferroic and magnetoelectric materials. *Nature* **442**, 759–765 (2006).
3. Ramesh, R. & Spaldin, N. A. Multiferroics: progress and prospects in thin films. *Nature Materials* **6**, 21–29 (2007).
4. Prellier, W., Singh, M. P. & Murugavel, P. The single-phase multiferroic oxides: from bulk to thin film. *J. Phys. Con. Mat.* **17**, R803–832 (2005).
5. Zheng, H. *et al*. Multiferroic $BaTiO_3$-$CoFe_2O_4$ nanostructures. *Science* **303**, 661–663 (2004).
6. Fiebig, M. Revival of the magnetoelectric effect. *J. Phys. D: Appl. Phys.* **38**, R123–R152 (2005).
7. Nan, C. W., Bichurin, M. I., Dong, S. X., Viehland, D. & Srinivasan, G. Multiferroic magnetoelectric composites: Historical perspective, status, and future directions. *J. Appl. Phys.* **103**, 031101 (2008).
8. Hill, N. A. Why are there so few magnetic ferroelectrics? *J. Phys. Chem. B* **104**, 6694–6709 (2000).
9. Catalan, G. & Scott, J. F. Physics and Applications of Bismuth Ferrite. *Adv. Mater.* **21**, 2463–2485 (2009).
10. Neaton, J. B., Ederer, C., Waghmare, U. V., Spaldin, N. A. & Rabe, K. M. First-principles study of spontaneous polarization in multiferroic $BiFeO_3$. *Phys. Rev. B* **71**, 014113 (2005).
11. Kimura, T. *et al*. Magnetic control of ferroelectric polarization. *Nature* **426**, 55–58 (2003).

12. Hur, N. *et al*. Electric polarization reversal and memory in a multiferroic material induced by magnetic fields. *Nature* **429**, 392–395 (2004).
13. Cheong, S.-W. & Mostovoy, M. Multiferroics: a magnetic twist for ferroelectricity. *Nature Materials* **6**, 13–20 (2007).
14. Tokura, Y. & Seki, S. Multiferroics with Spiral Spin Orders. *Adv. Mater.* **22**, 1554–1565 (2010).
15. Qi, X.-L., Hughes, T. L. & Zhang, S.-C. Topological field theory of time-reversal invariant insulators. *Phys. Rev. B* **78**, 195424 (2008).
16. Essin, A. M., Moore, J. E. & Vanderbilt, D. Magnetoelectric Polarizability and Axion Electrodynamics in Crystalline Insulators. *Phys. Rev. Lett.* **102**, 146805 (2009).
17. Pearson, G. L. & Brattain, W. H. History of Semiconductor Research, Proc. *IRE* **43**, 1794–1806 (1955).
18. Dharmatti, S. S. Anomalous Diamagnetism of Selenium. *Nature* **134**, 497 (1934).
19. Kahaly, M. U., Ghosh, P., Narasimhan, S. & Waghmare, U. V. Size dependence of structural, electronic, elastic, and optical properties of selenium nanowires: A first-principles study. *J. Chem. Phys.* **128**, 044718 (2008).
20. Lucovsky, G., Mooradian, A., Taylor, W., Wright, G. B. & Keezer, R. C. Identification of the fundamental vibrational modes of trigonal, α-monoclinic and amorphous Selenium. *Solid State Comm.* **5**, 113–117 (1967).
21. McCann, D. R. & Cartz, L. Bond distances and chain angle of hexagonal selenium at high pressure. *J. Appl. Phys.* **43**, 4473–4477 (1972).
22. Fischer, R. Absorption and electroabsorption of trigonal Selenium near the fundamental absorption edge. *Phys. Rev. B* **5**, 3087–3094 (1972).
23. Abdullaev, G. B., Asadov, Y. G. & Mamedov, K. P. in The Physics of Selenium and Tellurium edited by Cooper, W. C. (Pergamon, Oxford, 1969) p. 188.
24. Yazyev, O. V. Emergence of magnetism in graphene materials and nanostructures. *Rep. Prog. Phys.* **73**, 056501 (2010).
25. Hasan, M. Z. & Moore, J. E. Three-Dimensional Topological Insulators, in *Annual Review of Condensed Matter Physics,* Vol **2** (ed Langer, J. S.) 55–78 (Annual Reviews, 2011).
26. Soluyanov, A. A. & Vanderbilt, D. Computing topological invariants without inversion symmetry. *Phys. Rev. B* **83**, 235401 (2011).
27. Vanderbilt, D. Soft self-consistent pseudopotentials in a generalized eigenvalue formalism. *Phys. Rev. B* **41**, 7892–7895 (1990).
28. Mostovoy, M. Ferroelectricity in Spiral Magnets. *Phys. Rev. Lett.* **96**, 067601 (2006).
29. Fu, L. Topological Crystalline Insulators. *Phys. Rev. Lett.* **106**, 106802 (2011).
30. Dieulesaint, E. & Royer, D. Properties of piezoelectric Selenium and Selenium layers. *Ferroelectrics* **42**, 187–195 (1982).
31. Gerhard, L. Magnetoelectric coupling at metal surfaces. *Nature Nanotechnology* **5**, 792–797 (2010).
32. Giannozzi, P. *et al*. QUANTUM ESPRESSO: a modular and open-source software project for quantum simulations of materials. *J. Phys. Condens. Matter* **21**, 395502 (2009).
33. Perdew, J. P., Burke, K. & Ernzerhof, M. Generalized Gradient Approximation Made Simple. *Phys. Rev. Lett.* **77**, 3865–3868 (1996).
34. Cococcioni, M. & de Gironcoli, S. Linear response approach to the calculation of the effective interaction parameters in the LDA + U method. *Phys. Rev. B* **71**, 035105 (2005).
35. King-Smith, R. D. & Vanderbilt, D. Theory of polarization of crystalline solids. *Phys. Rev. B* **47**, 1651–1654 (1993).
36. Kohn, W. & Sham, L. J. Self-Consistent Equations Including Exchange and Correlation Effects. *Phys. Rev.* **140**, A1133–A1138 (1965).
37. Hartwigsen, C., Goedecker, S. & Hutter, J. Relativistic separable dual-space Gaussian pseudopotentials from H to Rn. *Phys. Rev. B* **58**, 3641–3662 (1998).
38. Gonze, X. *et al*. First-principles computation of material properties: the ABINIT software project. *Computational Materials Science* **25**, 478–492 (2002).
39. Goedecker, S. Fast radix 2, 3, 4, and 5 kernels for fast Fourier transformations on computers with overlapping Multiply-Add Instructions. *SIAM J. Sci. Comput.* **18**, 1605–1611 (1997).

Acknowledgments

We acknowledge Dr. A. Thamizhavel for useful suggestions regarding crystal growth, Dr. A. V. Gopal and Dr. M. Deshmukh for providing access to certain experimental facilities and Dr. S. B. Roy (RRCAT, Indore) for discussions. We thank Ms. B. Chalke and Mr. N. Kulkarni for their help with the electron microscopy and X-ray diffraction measurements, respectively.

Author contributions

A.P. carried out the experiments and analysed the data, S. Gohil participated in the Raman experiments; S.N.S. and U.V.W. carried out the theoretical calculations and analysis; S. Ghosh and P.A. planned the study; P.A. and U.V.W. wrote the paper with inputs from S. Ghosh and S.N.S.

Additional information

Supplementary information accompanies this paper at http://www.nature.com/scientificreports

Competing financial interests: The authors declare no competing financial interests.

How to cite this article: Pal, A. *et al*. Multiferroic Behavior in Elemental Selenium below 40 K: Effect of Electronic Topology. *Sci. Rep.* **3**, 2051; DOI:10.1038/srep02051 (2013).